

Phonon Bottleneck Effect Leads to Observation of Quantum Tunneling of the Magnetization and Butterfly Hysteresis Loops in $(\text{Et}_4\text{N})_3\text{Fe}_2\text{F}_9$

Ralph Schenker,^{1,*} Michael N. Leuenberger,^{2,†} Grégory Chaboussant,^{1,‡} Daniel Loss,^{2,§} and Hans U. Güdel^{1,¶}

¹*Department for Chemistry and Biochemistry, University of Bern, Freiestrasse 3, 3000 Bern 9, Switzerland*

²*Department of Physics and Astronomy, University of Basel, Klingelbergstrasse 82, 4056 Basel, Switzerland*

A detailed investigation of the unusual dynamics of the magnetization of $(\text{Et}_4\text{N})_3\text{Fe}_2\text{F}_9$ (Fe_2), containing isolated $[\text{Fe}_2\text{F}_9]^{3-}$ dimers, is presented and discussed. Fe_2 possesses an $S = 5$ ground state with an energy barrier of 2.40 K due to an axial anisotropy. Poor thermal contact between sample and bath leads to a phonon bottleneck situation, giving rise to butterfly-shaped hysteresis loops below 5 K concomitant with slow decay of the magnetization for magnetic fields H_z applied along the Fe–Fe axis. The butterfly curves are reproduced using a microscopic model based on the interaction of the spins with resonant phonons. The phonon bottleneck allows for the observation of resonant quantum tunneling of the magnetization at 1.8 K, far above the blocking temperature for spin-phonon relaxation. The latter relaxation is probed by AC magnetic susceptibility experiments at various temperatures and bias fields H_{DC} . At $H_{\text{DC}} = 0$, no out-of-phase signal is detected, indicating that at $T \geq 1.8$ K Fe_2 does not behave as a single-molecule magnet. At $H_{\text{DC}} = 1$ kG, relaxation is observed, occurring over the barrier of the thermally accessible $S = 4$ first excited state that forms a combined system with the $S = 5$ state.

PACS numbers: 75.45.+j, 75.50.Xx, 75.60.Ej, 75.60.Jk

I. INTRODUCTION

Among the most fascinating aspects of magnetism in recent years has been the discovery that the magnetic moment of individual molecules can give rise to magnetic hysteresis phenomena. Such systems lie at the interface between classical and quantum-mechanical regimes, and are thus of great fundamental as well as practical interest regarding future applications related to quantum computing.¹

Molecular clusters such as Mn_{12} ,^{2,3,4,5} Fe_8 ,⁶ and Mn_4 ⁷ have been found to exhibit hysteresis curves characterized by a remanence. They have been dubbed single-molecule magnets (SMMs) as each molecule behaves as a single-domain nanomagnetic particle. These high-spin systems possess an energy barrier $\Delta = |D_S|S^2$ for reversal of the direction of the magnetic moment (“spin”), arising from the combination of a large ground state total spin quantum number S with a uniaxial anisotropy (negative axial zero-field splitting parameter D_S). At $kT \ll \Delta$ the magnetization can be blocked and relaxes very slowly, giving rise to the hysteresis. Many SMMs such as Mn_{12} ^{3,4} and Fe_8 ⁶ exhibit quantum tunneling of the magnetization (QTM) through the energy barrier.

Alternatively, a different type of hysteresis lacking a remanence has been observed for $[\text{Fe}(\text{salen})\text{Cl}]_2$ ⁸ and more recently for the $S = 1/2$ spin cluster V_{15} ⁹ as well as the antiferromagnetically coupled ($S = 0$) ferric wheels Fe_6 ¹⁰ and Fe_{12} .¹¹ In these low-spin systems the ground state does not possess a magneto-structural energy barrier for the reversal of the total spin.¹² Instead, the hysteresis is created by dynamically driving the spin system out of thermal equilibrium due to insufficient thermal contact of the sample with the heat bath, thereby causing a phonon bottleneck (PB) effect. It possesses a characteristic butterfly shape that arises from a fast spin reversal at

the field value where the anticrossing of the two lowest-energy levels occurs.^{9,10} Generally, the magnitude of the anticrossing level splitting determines the quantum dynamics of the spins. In the low-spin systems, this splitting is relatively large ($\geq 10^{-3}$ K), allowing for fast spin reversal yielding the butterfly shape. On the other hand, in high-spin systems the tunnel splitting between the lowest levels of typically $\leq 10^{-6}$ K renders QTM too slow for allowing a butterfly-shaped hysteresis. Therefore it was previously argued that butterfly hystereses are not expected for high-spin systems.⁹ Nevertheless, recently for the SMM Mn_9 a butterfly hysteresis caused by the PB effect was reported above the blocking temperature for SMM behavior, but no analysis was offered.¹³ Very little is known to date about the physics of this phenomenon in spin systems with an energy barrier. However, such information is of particular interest as the presence of the barrier principally enables these clusters to behave as single-molecule magnets.

The tri- μ -fluoro bridged $[\text{Fe}_2\text{F}_9]^{3-}$ dimer molecule in the compound $(\text{Et}_4\text{N})_3\text{Fe}_2\text{F}_9$ (Et_4N = tetraethylammonium), abbreviated Fe_2 , possesses an $S = 5$ ground state with an energy barrier of 2.40 K for spin reversal (Fig. 1).¹⁴ As reported previously,¹⁵ Fe_2 exhibits slow relaxation of the magnetization and magnetic hysteresis below 5 K. The hysteresis adopts a butterfly shape tied up at $H_z = 0$ despite the presence of the energy barrier. The observation of QTM prompted us to ascribe these phenomena to the unusually slow relaxation of a single-molecule magnet.¹⁵ However, meanwhile additional data have provided compelling evidence that the observed relaxation depends on the thermal insulation of the sample.

Here we present a detailed study on the magnetic properties of Fe_2 . The earlier findings are reinterpreted in terms of the phonon bottleneck. A microscopic model based on the rapid absorption/emission of reso-

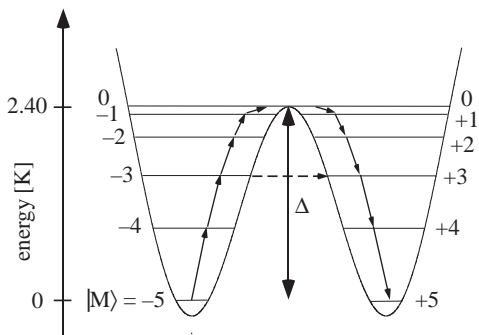


FIG. 1: Double-well potential of the $S = 5$ ground state of Fe_2 with the energy barrier $\Delta = |D_S S^2| = 2.40$ K. Full and broken arrows indicate spin-phonon and QTM transitions, respectively.

nant phonons is developed that allows for an accurate reproduction of the observed hysteresis curves. Finally, alternating-current (AC) magnetic susceptibility data reflecting the fast relaxation behavior of Fe_2 unaffected by the phonon bottleneck effect are presented and discussed.

II. EXPERIMENTAL

Needle-shaped single crystals of $(\text{Et}_4\text{N})_3\text{Fe}_2\text{F}_9$ (Fe_2) up to 5 mm in length were prepared according to Ref. 14. The dimer symmetry is exactly C_{3h} with the threefold axis lying parallel to the hexagonal crystal axis c .¹⁶ The intradimer $\text{Fe}\cdots\text{Fe}$ distance is 2.907 Å. The dimer molecules are well separated from each other, leading to interdimer $\text{Fe}\cdots\text{Fe}$ distances of at least 8 Å, thus making interdimer interactions extremely inefficient.

Samples for magnetic experiments were prepared as follows: To prevent hydrolyzation, samples were prepared in a drybox under a nitrogen atmosphere. All the crystals were perfectly transparent, indicating that no hydrolysis occurred. A single crystal of 2.46 mg (sample **A**) was sealed in a glass tube under N_2 in $\mathbf{H} \parallel c$ (H_z) orientation. At liquid helium temperatures, the N_2 is frozen out and its vapor pressure inside the glass tube becomes very low, leading to a poor heat contact of the crystal with its surroundings. Alternatively, three single crystals (total mass 48 mg) were embedded in Apiezon grease in a dried gelatine capsule to yield a sample (**B**) with improved heat contact. Alternating-current (AC) magnetic susceptibility measurements were performed both on sample **B** and on a polycrystalline powder sample (**C**) of 25 mg made of crushed single crystals, sealed in a dried gelatine capsule.

Magnetic measurements were carried out using a Quantum Design MPMS-XL-5 Superconducting Quantum Interference Device (SQUID) magnetometer equipped with a 5 T magnet. The oscillation frequency of the AC field was varied between 10 and 1488 Hz at an AC field strength of 1 G. All data were corrected for the diamagnetism of the atoms using Pascal's constants.

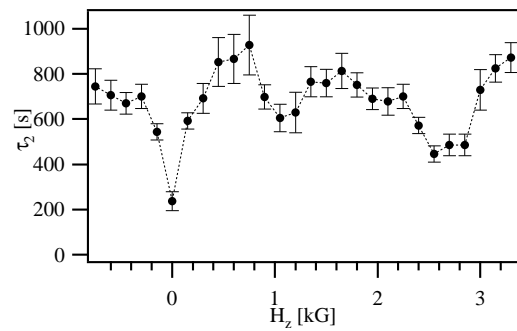


FIG. 2: Dependence of the relaxation time τ_2 on H_z at $T = 1.8$ K with error (3σ). The dotted line is a guide to the eyes.

III. RESULTS

A. Relaxation of the Magnetization

Magnetization relaxation experiments were performed using sample **A** in $\mathbf{H} \parallel c$ orientation at fixed values of H_z and bath temperature T , after saturation at 30 kG and subsequent quick (≈ 150 G/s) reduction to the indicated H_z value. Relaxation times τ_2 were extracted from least-squares fits of a single-exponential law to the relaxation curves for various values of H_z . The resulting field dependence of τ_2 at 1.8 K (Fig. 2) reveals that τ_2 varies between 240 s at $H_z = 0$ and 870 s at 3.3 kG. Importantly, 3 distinctive dips are observed at $H_z = 0$, 1.1, and 2.7 kG.

B. Butterfly Hysteresis Curves

Magnetization measurements at fixed T were performed in $\mathbf{H} \parallel c$ (H_z) orientation by varying H_z from +50 kG to -50 kG and back to +50 kG. For the crystal embedded in Apiezon grease (sample **B**), the magnetization follows the thermal equilibrium curve (asterisks in Fig. 3). Alternatively, for a crystal mounted in the glass tube (sample **A**), it features a butterfly-shaped hysteresis loop characterized by two distinct features: (i) the magnetization at $H_z = 0$ is zero, and (ii) near $H_z = 0$ the magnitudes of both the magnetization detected while approaching $H_z = 0$ and the one while receding from it are larger than the thermal equilibrium value (inset of Fig. 3). As this butterfly hysteresis is perfectly centrosymmetric, further data in Fig. 4 show only the positive wings. The hysteresis effect decreases with increasing T , vanishing above 5 K (Fig. 4). Reduction of the sweeping rate from $\Gamma \approx 3$ G/s to ≈ 1 G/s¹⁷ narrows the breadth of the wings (Fig. 2 in Ref. 15), suggesting that for a substantially smaller value of Γ the magnetization would follow the thermal equilibrium curve (dashed line in Fig. 3).

A drastic change in the magnetization curve of sample **A** occurs upon a very fast sweep of the magnetic field.

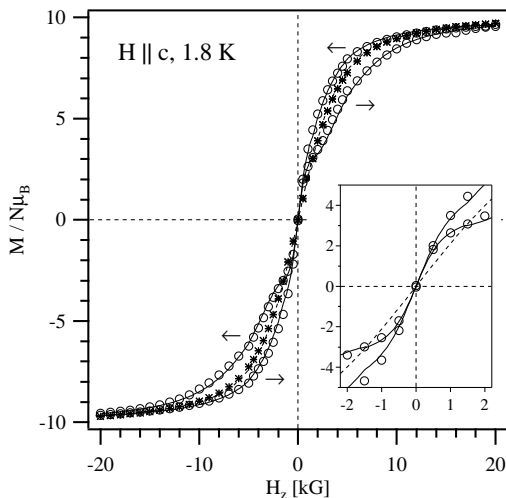


FIG. 3: Hysteresis of the magnetization of Fe₂ single crystals (open circles: sample **A**, asterisks: sample **B**) at 1.8 K obtained with $\Gamma \approx 3$ G/s. The arrows indicate the direction of the measurement. The solid lines are calculated using the resonant-phonon model (Sec. IV C). The dashed line represents the thermal equilibrium curve calculated with $J = -2.23$ K, $D = -0.215$ K, and $g = 2.00$.¹⁴ The inset highlights the region close to $H_z = 0$.

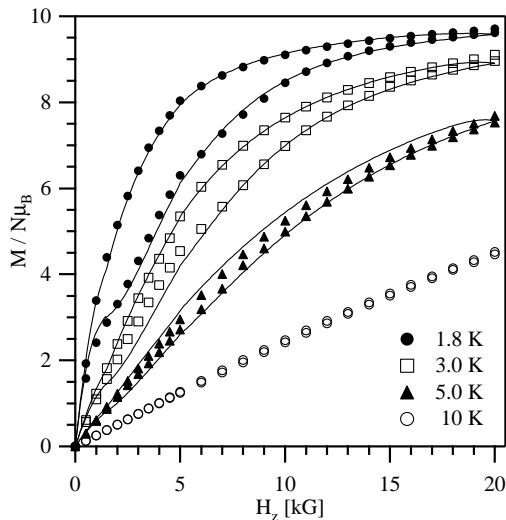


FIG. 4: Positive wings of the butterfly hysteresis of the magnetization of a single crystal (sample **A**) for $\mathbf{H} \parallel c$ orientation at different temperatures as indicated with $\Gamma \approx 3$ G/s. The solid lines are calculated using the resonant-phonon model (Sec. IV C).

Fig. 5 shows magnetization data obtained as follows: after saturation at +30 kG, the field was quickly ($\Gamma \approx 150$ G/s) reduced to the given values of H_z including negative ones, and the magnetization was measured within 50 s after reaching H_z . During such a fast sweep, the magnetization essentially switches from positive to negative saturation upon crossing $H_z = 0$.

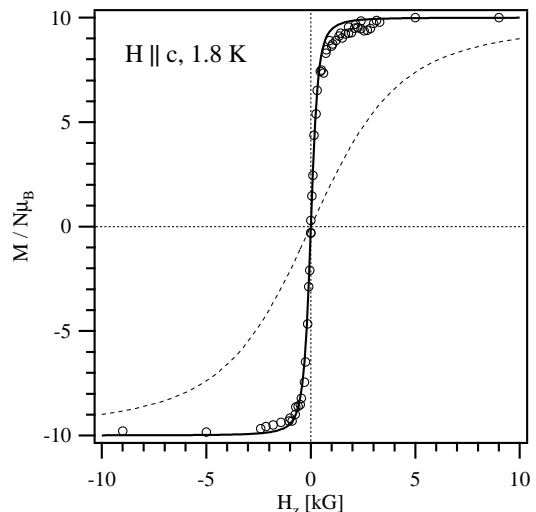


FIG. 5: Magnetization data (sample **A**) at 1.8 K obtained as follows: after saturation at +30 kG the field was quickly ($\Gamma \approx 150$ G/s) reduced to the given H_z values including negative ones, and the magnetization was measured within 50 s after reaching H_z . The solid line is the adiabatic curve calculated using the resonant-phonon model described in the text with $H_{\text{eff},x} = 350$ G, while the dashed line represents the thermal equilibrium curve.

C. AC Magnetic Susceptibility

To complement our studies on the magnetization relaxation in Fe₂, alternating-current (AC) susceptibility experiments were performed on both the polycrystalline sample **C** and the single crystals in $\mathbf{H}_{\text{AC}} \parallel \mathbf{H}_{\text{DC}} \parallel c$ orientation embedded in Apiezon grease (sample **B**). H_{DC} denotes a static bias field and for sample **B** corresponds to H_z . With respect to relaxation, no significant differences were found between the two samples.¹⁸ Experiments were conducted within a temperature range $1.8 \leq T \leq 15$ K with an amplitude of $H_{\text{AC}} = 1$ G and oscillation frequencies $10 \leq \nu \leq 1488$ Hz. Importantly, an out-of-phase susceptibility (χ'') was observed only upon application of an additional static magnetic field H_{DC} .

Figure 6 shows the frequency dependence of χ'' vs T at selected static fields of 1 kG and 5 kG using the polycrystalline sample. As ν is reduced from 1488 Hz to 100 Hz, at 1 kG the peak maximum T_{max} shifts from 5.2 K to 2.45 K, and further reduction to 10 Hz causes it to shift below 1.8 K. At 5 kG the situation is similar. In both cases T_{max} increases with ν , from which the temperature dependence of the relaxation rate $1/\tau = 2\pi\nu$ is derived, shown in Fig. 7 as Arrhenius plots of $\ln(1/\tau)$ versus $1/T_{\text{max}}$. At $H_{\text{DC}} = 1$ kG the data follow the Arrhenius law

$$\frac{1}{\tau} = \frac{1}{\tau_0} \cdot e^{-\Delta E/kT}, \quad (1)$$

where $1/\tau_0 = 1.0 \times 10^5 \text{ s}^{-1}$ is the intrinsic relaxation rate and $\Delta E = 12.6 \pm 0.2$ K the kinetic energy barrier. At

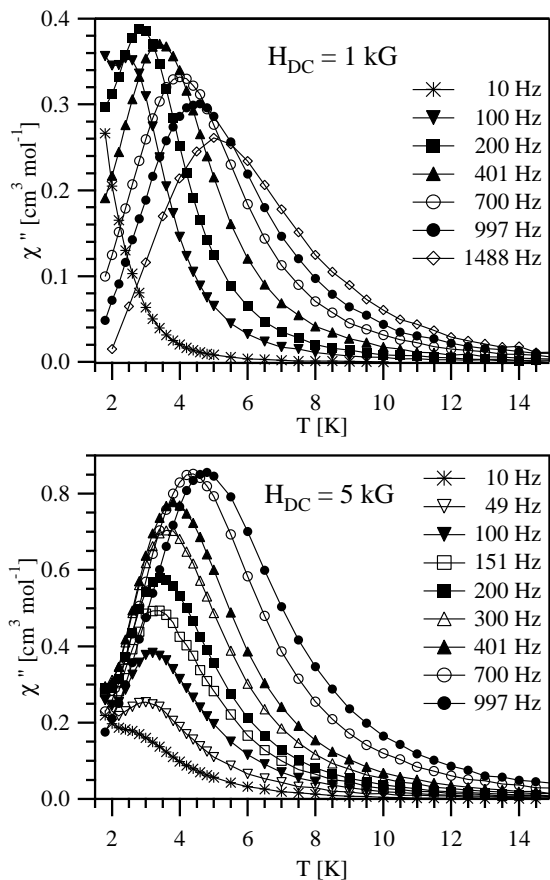


FIG. 6: Out-of-phase AC susceptibility χ'' vs T at $H_{DC} = 1$ kG (top) and 5 kG (bottom) for a polycrystalline sample (C) of Fe_2 in a 1 G AC field oscillating with the indicated frequencies ν .

$H_{DC} = 5$ kG, however, the temperature dependence of $1/\tau$ is linear (inset of Fig. 7).

Interestingly, for higher frequencies, χ'' is considerably larger at 5 kG than at 1 kG. Indeed, we observed that for $\nu = 997$ Hz, χ'' increases linearly with H_{DC} below 2.5 kG and appears to level off at higher fields (not shown).

IV. ANALYSIS AND DISCUSSION

A. Phonon Bottleneck Effect

In H_z orientation, Fe_2 single crystals in a glass tube (sample A) exhibit slow magnetization relaxation on the timescale of $10^2 - 10^3$ s, whereas crystals embedded in Apiezon grease (sample B) do not. Obviously this relaxation depends on the degree of thermal insulation of the sample. Poor thermal contact between the crystal and the heat bath (as for sample A) is well known to lead to the macroscopic observation of the phonon bottleneck (PB).^{19,20} Also, the butterfly hysteresis loops observed for Fe_2 closely resemble those recently reported for the

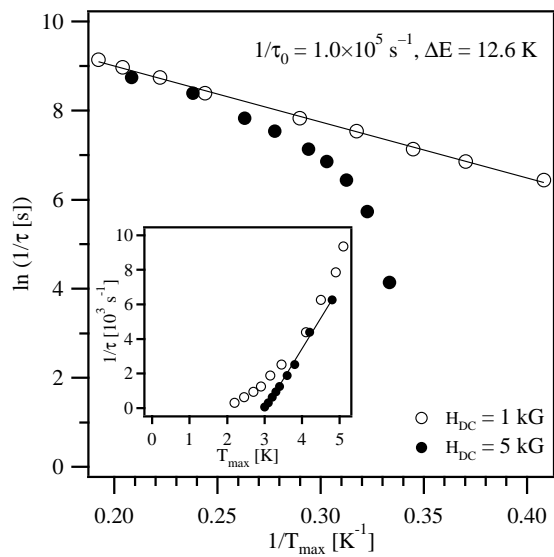


FIG. 7: Temperature dependence of the AC χ'' relaxation rate $1/\tau = 2\pi\nu$ shown as an Arrhenius plot ($\ln 1/\tau$ vs $1/T_{\max}$) as extracted from the data in Fig. 6. The solid line represents a least-squares fit of the $H_{DC} = 1$ kG data to the Arrhenius law (Eq. 1), yielding the prefactor $1/\tau_0$ and the kinetic energy barrier ΔE as indicated. The inset shows the same data on a linear scale. Note the linear dependence of $1/\tau$ on T_{\max} for the $H_{DC} = 5$ kG data.

spin clusters V_{15} ,⁹ Fe_6 ,¹⁰ and Fe_{12} ¹¹ that have been attributed to this effect. Thus, it is the phonon bottleneck that causes the observed slow relaxation in Fe_2 .

The energy exchange between the spin system and the bath occurs via the phonons in the crystal. The PB describes the fact that at low temperatures the number of spins is much larger than the number of available phonons. Thermodynamically speaking, the heat capacity of the spins C_s far exceeds that of the phonons C_p .²¹

$$b = \frac{C_s + C_p}{C_p} \approx \frac{C_s}{C_p} \gg 1, \quad (2)$$

such that $b \approx 10^4 - 10^6$.²¹ The observable relaxation time is²¹

$$\tau_2 = \tau_{\text{sp}} + b\tau_{\text{pb}}, \quad (3)$$

with τ_{sp} and τ_{pb} denoting the spin-phonon and phonon-bath relaxation times, respectively. Importantly, upon poor thermal contact between the phonons and the bath, τ_{pb} becomes very large such that $\tau_2 \approx b\tau_{\text{pb}}$, thus rendering the bottleneck macroscopically observable. In a PB situation, the initial rapid energy transfer from the spins to the phonons quickly heats the latter to the temperature of the former, such that these phonons become in resonance with the energy differences between individual $|M\rangle$ levels.²¹ Thus, the spins and these resonant phonons form a single coupled system that can only very slowly exchange energy with the bath, leading to the observed magnetization relaxation.

B. Quantum Tunneling of the Magnetization in Fe₂

A very important result of our studies is the observation of dips in the field dependence of τ_2 (Fig. 2). Such dips are often observed in single-molecule magnets such as Mn₁₂,^{3,4} and interpreted as fingerprints for resonant QTM at the respective field values, which lowers the relaxation time. In the case of Fe₂, the dependence of τ_2 on H_z appears very intriguing as the slow relaxation arises from the weak thermal contact between the sample and the bath, which hardly depends on H_z . However, since a tunneling pathway represents a bypass, QTM occurs in parallel to thermal relaxation involving phonons.²³ Thus, its presence can significantly alter the observed relaxation time τ_2 even if the latter is dominated by the phonon-bath relaxation. Indeed, recently Chiorescu et al. reported magnetization relaxation data on the V₁₅ spin cluster under virtually adiabatic conditions analogous to our situation for Fe₂.²² The authors found that around $H_z = 0$ the measured phonon-bath relaxation time τ_2 dropped by a factor of 2–3 due to the level anticrossing.

In the C_{3h} dimer symmetry of Fe₂,¹⁶ the full anisotropy Hamiltonian including higher-order terms reads²¹

$$\mathcal{H}_{\text{ani}} = D_S \left[\hat{S}_z^2 - \frac{1}{3}S(S+1) \right] + B_4^0 \hat{O}_4^0 + B_6^0 \hat{O}_6^0 + B_6^6 \hat{O}_6^6, \quad (4)$$

where $\hat{O}_4^0 = 35\hat{S}_z^4 - 30S(S+1)\hat{S}_z^2 + 25\hat{S}_z^2 - 6S(S+1) + 3\hat{S}^2(S+1)^2$, $\hat{O}_6^0 = 231\hat{S}_z^6 - 315S(S+1)\hat{S}_z^4 + 735\hat{S}_z^4 + 105S^2(S+1)^2\hat{S}_z^2 - 525S(S+1)\hat{S}_z^2 + 294\hat{S}_z^2 - 5S^3(S+1)^3 + 40S^2(S+1)^2 - 60S(S+1)$, and $\hat{O}_6^6 = (S_+^6 + S_-^6)/2$. The $B_6^6 \hat{O}_6^6$ term mixes wavefunctions with $\Delta M = \pm 6$, allowing for resonant tunneling at $H_z = 0$ between the $|M\rangle$ levels $-3/+3$ (Fig. 1) and at applied fields when the $-2/+4$ and $-1/+5$ levels cross. For $B_4^0 = B_6^0 = 0$, the fields $H_z^{MM'}$ at which resonant tunneling is expected for the $S = 5$ state in Fe₂ are given by²³

$$H_z^{MM'} = -\frac{nD_5}{g\mu_B} = n \cdot 714 \text{ G}, \quad (5)$$

where $n = M + M'$ is an integer ranging from 0 to 9. Resonant tunneling may therefore occur for $n = 0, 2$, and 4 at field values of $H_z = 0, 1.4$, and 2.85 kG, corresponding to the $|M\rangle$ level crossings $-3/+3$ (Fig. 1), $-2/+4$, and $-1/+5$, respectively. Therefore we can expect three dips in the field dependence of τ_2 , in agreement with the experimental data in Fig. 2. The dips are centered at $0, \approx 1.1$, and ≈ 2.7 kG instead of $0, 1.4$, and 2.85 kG, suggesting nonzero values for B_4^0 and B_6^0 in Eq. (4). Thus the observed dips in Fig. 2 are consistent with quantum tunneling processes in Fe₂ at 1.8 K. However, QTM does not appear to be dominant in Fe₂ as the drop of τ_2 due to QTM compared to pure thermal relaxation at nonresonant fields is only on the order of 25 % for $H_z = 1.1$ and 2.7 kG and 75 % for $H_z = 0$ (Fig. 2). This behavior is in contrast to the situation in, e.g., Mn₁₂ in absence of a PB effect, where upon QTM the relaxation time decreases by

several orders of magnitude.^{3,4} We ascribe this difference to the fact that in Fe₂ the tunneling is phonon-assisted and thus slowed down by the bottleneck effect.

Importantly, our results on Fe₂ demonstrate that quantum tunneling of the magnetization can be observed even though the relaxation monitored mainly represents the phonon-bath relaxation. By creating a PB situation, QTM is observed at 1.8 K, i.e. far above the blocking temperature for magnetization relaxation reflecting intrinsic spin-phonon relaxation.

C. Modeling the Butterfly Hysteresis Loops

The butterfly hysteresis reflects a spin reversal at $H_z = 0$. For [Fe(salen)Cl]₂, it was reproduced using a phenomenological, thermodynamic model,⁸ whereas for V₁₅⁹ and Fe₆¹⁰ a dissipative two-level model with a level anticrossing was employed. In contrast to these systems, for Fe₂ the presence of 11 levels and the energy barrier for spin reversal in the $S = 5$ state complicate matters considerably. As QTM is significant but not dominant in Fe₂ (Sec. IV B), it is likely that the spin reversal is predominantly achieved by thermal activation over the barrier. To reproduce the butterfly shape of the hysteresis curves in Fe₂, we thus decided to employ a novel, microscopic model that explicitly accounts for the barrier. Note that although this model is based on the absorption and emission of resonant phonons, it does not exclude the possibility of QTM.

As the resonant phonons cannot relax with the phonon bath to regain thermal equilibrium, they produce coherent transitions of the spins on both sides of the barrier at all values of H_z ; however, only at $H_z = 0$ these transitions lead to a change in the macroscopically observed magnetization. In the adiabatic limit the total energy of the combined system remains constant. Therefore the number of the absorptions and emissions has to be equal, leading to the spin flip at $H_z = 0$. The coherent spin transitions $\Delta M = \pm 1$ occur between all the spin levels $|M\rangle$, $M = -5, \dots, 5$. They can be mimicked mathematically by effective oscillating transversal magnetic fields $H_{\text{eff},x}(t) = H_{\text{eff},x} \sum_{-5}^{+5} \cos(\omega_{M,M+1}t)$. In its simplest form, the resulting effective Hamiltonian for the $S = 5$ state of Fe₂ in $\mathbf{H} \parallel c$ orientation reads²⁴

$$\mathcal{H}_{\text{eff}} = D\hat{S}_z^2 + g\mu_B H_{\text{eff},x}(t)\hat{S}_x + g\mu_B H_z \hat{S}_z. \quad (6)$$

Following the derivation of the Hamiltonian in the generalized rotating frame²⁵ (details see Appendix), we obtain

$$\mathcal{H}_{\text{eff}}^{\text{rot}} = g\mu_B H_{\text{eff},x} \hat{S}_x + g\mu_B H_z \hat{S}_z. \quad (7)$$

The levels $|m\rangle = -5, \dots, 5$ correspond to the combined spin+phonons system. Their response $\mathcal{H}_{\text{eff}}^{\text{rot}}$ is shown in Fig. 8 for $H_{\text{eff},x} = 350$ G. Within about $-0.5 \leq H_z \leq +0.5$ kG, they become strongly mixed, and at $H_z = 0$ they are equidistantly split by $10g\mu_B H_{\text{eff},x} = 0.47$ K. Note that in the generalized rotating frame the energy

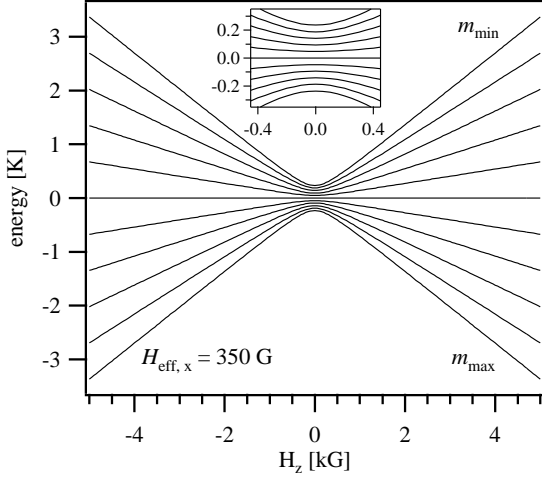


FIG. 8: Dependence of the 11 energy levels $|m\rangle$ defined by $\mathcal{H}_{\text{eff}}^{\text{rot}}$ (Eq. 7) on H_z , arising from the resonant phonons ($H_{\text{eff},x} = 350$ G). The inset highlights the anticrossing at $H_z = 0$.

of a given resonant phonon is added to the energy of a given $|M\rangle$ level.²⁵ Consequently, the energy difference to the adjacent level and hence the entire energy barrier disappear. Therefore, the resonant phonons provide an efficient way to overcome this barrier, leading to the butterfly-shaped hysteresis.

In the adiabatic limit corresponding to the data in Fig. 5 obtained upon a fast ($\Gamma \approx 150$ G/s) sweep, the combined spin+phonons system remains decoupled from the bath. Thus the magnetization essentially switches from positive to negative saturation upon crossing $H_z = 0$, indicating that during the entire sweep only the lowest level in Fig. 8 is populated. Consequently, $M(H_z) \propto d\varepsilon_{m_{\text{max}}}/dH_z$, where $\varepsilon_{m_{\text{max}}}$ is the energy of the lowest-energy level defined by $\mathcal{H}_{\text{eff}}^{\text{rot}}$ (Fig. 8). With $H_{\text{eff},x} = 350$ G the agreement with the experimental data is excellent (Fig. 5), thus lending credence to our model, in which $H_{\text{eff},x}$ is the *only* adjustable parameter. The range $-0.5 \leq H_z \leq +0.5$ kG in which the spin reversal occurs (Fig. 5) mirrors the zone in which the levels are highly mixed (Fig. 8). Thus it directly depends on the magnitude of $H_{\text{eff},x}$ by $(dM/dH_z)_{H_z \rightarrow 0} \propto 1/H_{\text{eff},x}$.

In nonadiabatic situations with a slow sweeping rate, corresponding to the butterfly hystereses in Figs. 3 and 4, the combined system is able to partially relax to thermal equilibrium during the measurement. Thus, the fast reversal process has to be combined with the slow relaxation process. Inside a region around $H_z = 0$ we apply the resonant phonon model (*vide supra*) with energy levels ε_m of the combined system to account for the fast spin reversal. Additionally, the slow sweeping rate together with the weak phonon-bath coupling gives rise to the presence of a small number of nonresonant or thermal phonons, which allows for the slow relaxation of the combined system to the bath. Thus, at $H_z = 0$ the relaxation

time becomes²³

$$\tau_{\text{in}} = \frac{1}{1 + e^{(\varepsilon_{m_{\text{min}}} - \varepsilon_{m_{\text{max}}})/kT}} \sum_{j=1}^{2S} \frac{e^{(\varepsilon_{m_j} - \varepsilon_{m_{\text{max}}})/kT}}{W_{m_j}^{m_{j+1}}}, \quad (8)$$

where $m_{\text{min}} = m_1$ and $m_{\text{max}} = m_{2S+1}$. The spin-thermal phonon transition rates read

$$\begin{aligned} W_{m_j}^{m_{j+1}} &= \frac{g_0^2 S_{m_j}^{m_{j+1}}}{48\pi\rho v^5 \hbar^4} \frac{(\varepsilon_{m_{j+1}} - \varepsilon_{m_j})^3}{e^{(\varepsilon_{m_{j+1}} - \varepsilon_{m_j})/kT} - 1} \\ &= \frac{g_0^2 S_{m_j}^{m_{j+1}}}{24\pi\rho v^5 \hbar^4} \frac{(\varepsilon_{m_{j+1}} - \varepsilon_{m_j})^3 e^{(\varepsilon_{m_j} - \varepsilon_{m_{j+1}})/2kT}}{\sinh[(\varepsilon_{m_{j+1}} - \varepsilon_{m_j})/2kT]}, \end{aligned} \quad (9)$$

where g_0 is the spin-thermal phonon interaction parameter, $\rho = 1.36 \times 10^3$ g/cm³ the mass density,¹⁶ v the sound velocity, and $S_{m_j}^{m_{j+1}} = (S - M_j)(S + M_j + 1)(2M_j + 1)^2$ in the quantization axis defined by $\mathbf{H}_{\text{eff},x}$ (note that $H_z = 0$).²⁶ Considering only transitions between the two lowest levels, τ_{in} can be approximated by

$$\begin{aligned} \tau_{\text{in}} &\approx \frac{1}{1 + e^{(\varepsilon_{m_{\text{min}}} - \varepsilon_{m_{\text{max}}})/kT}} \frac{e^{(\varepsilon_{m_{2S}} - \varepsilon_{m_{\text{max}}})/kT}}{W_{m_{2S}}^{m_{\text{max}}}} \\ &= \frac{\sinh[(\varepsilon_{m_{\text{max}}} - \varepsilon_{m_{2S}})/2kT]}{1 + e^{(\varepsilon_{m_{\text{min}}} - \varepsilon_{m_{\text{max}}})/kT}} \frac{e^{(\varepsilon_{m_{2S}} - \varepsilon_{m_{\text{max}}})/2kT}}{\gamma_{m_{2S}}^{m_{\text{max}}}}, \end{aligned} \quad (10)$$

where $\gamma_{m_{2S}}^{m_{\text{max}}} = g_0^2 S_{m_{2S}}^{m_{\text{max}}} (\varepsilon_{m_{\text{max}}} - \varepsilon_{m_{2S}})^3 / 24\pi\rho v^5 \hbar^4 = 810g_0^2 (g\mu_B H_{\text{eff},x})^3 / 24\pi\rho v^5 \hbar^4$ at $H_z = 0$.²⁶ Notably, as for a two-level system $m_{2S} = m_{\text{min}}$, this equation shows the well-known tanh behavior for the relaxation time of a two-level system.²¹

A general relaxation time τ_{out} was chosen to account for the phonon bottleneck effect outside the region around $H_z = 0$. The time evolution of the magnetization is given by $\dot{M}(t) = -[M(t) - M_{\text{eq}}(H_z(t))]/\tau$ that for small values of Γ yields

$$M(t) = M_{\text{eq}} + (M_{\text{sat}} - M_{\text{eq}})e^{-t/\tau}, \quad (11)$$

where $M_{\text{sat}} = M(H_{\text{sat}})$ and $M_{\text{eq}} = M_{\text{eq}}(H_z)$ denote the magnetizations at saturation and thermal equilibrium, respectively. $H_z(t) = H_{\text{sat}} + \Gamma t$ was swept from $H_z = H_{\text{sat}} = -10.0$ kG to $+10.0$ kG. $\tau = \tau_{\text{in}}$ for $|H_z| \leq 1.5$ kG and $\tau = \tau_{\text{out}}$ for $|H_z| > 1.5$ kG. The value of H_z that marks the border between the two regimes is defined by the magnitude of $H_{\text{eff},x}$.

The butterfly hysteresis in Fig. 3 was best reproduced with $\tau_{\text{in}} = 2100$ s, whose temperature dependence turned out to be insignificant below 10 K. Assuming a realistic sound velocity of $v = 1400$ m/s,²³ this value corresponds to $g_0 = 0.72$ mK, i.e. about 3 orders of magnitude smaller than the values reported for Mn₁₂²³ and Fe₈²⁷. This low value for g_0 in Fe₂ arises from the fact that the number of thermal phonons is very small due to the weak phonon-bath coupling in our experiments. Hence, it does not necessarily reflect a weak spin-phonon interaction.

$\tau_{\text{out}} = 550$ s as obtained from the fit is in overall reasonable agreement with the experimental values for τ_2 deduced from the magnetization relaxation curves (Fig. 2). Importantly, $\tau_{\text{in}} > \tau_{\text{out}}$, which leads to the typical features of a butterfly hysteresis loop. The resonant phonon field is $H_{\text{eff},x} = 1$ kG, which is about three times larger than the value obtained from the analysis of the data in Fig. 5, indicating that $H_{\text{eff},x}$ depends on the sweeping rate. The best fit was obtained with sweeping rates of 2.5 G/s for $|H_z| \leq 5$ kG and 3.3 G/s for $|H_z| > 5$ kG, i.e. in very good agreement with the experimental values.¹⁷ To fit the butterfly hystereses at 3 and 5 K (Fig. 4), τ_{out} and $H_{\text{eff},x}$ were multiplied with the Boltzmann factor $e^{\Delta(1/kT_1 - 1/kT_2)}$, where $T_2 = 1.8$ K and $T_1 = 3$ K or 5 K. The decrease of τ_{out} and $H_{\text{eff},x}$ with increasing T reflects the fact that (i) the coherence and thus relevance of the resonant phonons decreases, and (ii) the phonon-bath coupling increases.

D. Intrinsic Spin-Phonon Dynamics

Insight into the intrinsic spin-phonon relaxation properties of Fe_2 unaffected by the PB is provided by the AC susceptibility experiments on samples with a good thermal contact with the bath. The absence of a PB situation is confirmed by the identical relaxation rates $1/\tau$ found for single-crystalline (sample **B**) and powder samples (sample **C**) at given values of H_{DC} , as otherwise $1/\tau$ would increase with the size of the crystallites as phonon scattering at the boundary walls decreases.^{28,29}

With an $S = 5$ ground state and an energy barrier of $\Delta = 2.40$ K for spin reversal, Fe_2 features the principal requirements necessary for exhibiting SMM behavior. However, from the absence of a χ'' signal at $H_{\text{DC}} = 0$ we conclude that Fe_2 does not behave as an SMM at $T \geq 1.8$ K. Obviously at these temperatures the relaxation over the small barrier is beyond the detectable range; presumably the blocking temperature for SMM relaxation lies in the mK region. However, by applying a static field H_{DC} , strong χ'' features are readily observed. We ascribe this difference to the fact that at $H_{\text{DC}} \neq 0$, phonons absorbed on one side of the barrier can no longer resonate with those emitted on the other side, rendering the relaxation considerably less efficient.

The relaxation rate $1/\tau$ is temperature dependent, indicating that the relaxation occurs via a thermal activation process. At $H_{\text{DC}} = 1$ kG, the temperature dependence of $1/\tau$ follows the Arrhenius law (Fig. 7), thus suggesting an Orbach process.²¹ This behavior is typically observed for SMMs, and often the value for ΔE is regarded as a lower limit for the SMM barrier height (note that χ'' features at $H_{\text{DC}} \neq 0$ have been reported for a few SMMs including Mn_4 ,⁷ V_4 ,³⁰ and Mn_{12} ;^{31,32} for V_4 , the χ'' signal was observed only at $H_{\text{DC}} \neq 0$). However, in Fe_2 the kinetic energy barrier of $\Delta E = 12.6 \pm 0.2$ K is 4 times larger than the thermodynamic barrier of the $S = 5$ state at 1 kG, $\Delta = 3.1$ K (Fig. 9). Importantly,

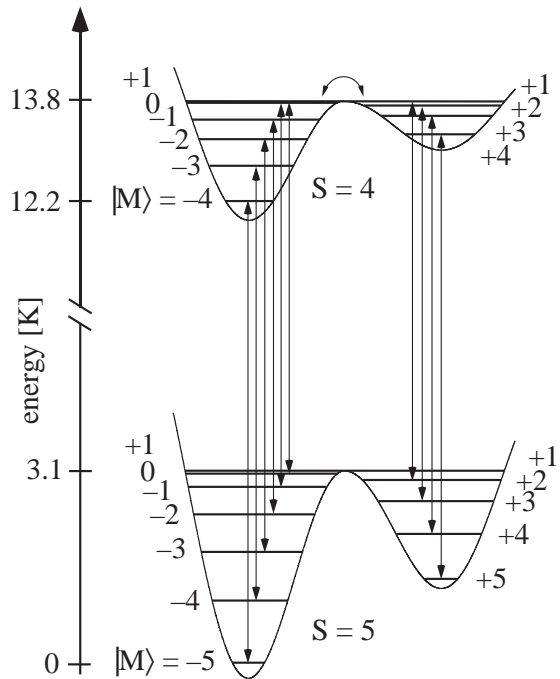


FIG. 9: Double well potential for a bias field of $H_{\text{DC}} = 1$ kG. The arrows indicate individual $\Delta S = \Delta M \pm 1$ spin-phonon transitions within the combined $S = 5$, $S = 4$ spin system and illustrate a likely scenario for spin-phonon relaxation.

this value lies close to the exchange splitting between the $S = 5$ and the $S = 4$ states of only 11.2 K¹⁴ (Fig. 9 shows the anisotropy and Zeeman splittings of these states at $H_{\text{DC}} = 1$ kG). This similarity hints toward a relaxation process involving transitions to the $S = 4$ state (Fig. 9). While the time-averaged level populations of the spin system are defined by the Boltzmann statistics, the oscillating field induces steady-state spin-phonon transitions on both sides of the barrier in an attempt to achieve thermal equilibrium. At $T_{\text{max}} \approx 4$ K, the $S = 4$ state is populated by about 5%, and so is the phonon energy spectrum. Assuming a Debye model, at 4 K the density of phonon states suitable for, e.g., an $|S, M\rangle = |5, -5\rangle \rightarrow |4, -4\rangle$ transition is about two orders of magnitude higher than that for a $|5, -5\rangle \rightarrow |5, -4\rangle$ transition, resulting in a strongly increased number of available thermal phonons for spin-phonon transitions. Also, at 4 K all the $S = 5$ levels are highly populated. Consequently, a relaxation process involving $\Delta S = \pm 1$ rather than $\Delta S = 0$ transitions (Fig. 9) becomes favorable. Therefore we postulate that the $S = 5$ and $S = 4$ states form a combined system in which the relaxation occurs from the $S = 5$ state over the barrier of the $S = 4$ state. The effective energy barrier is then 13.8 K and 12.5 K for transitions from the deeper to the shallower well and *vice versa*, respectively, in good agreement with the kinetic energy barrier $\Delta E = 12.6 \pm 0.2$ K. This agreement further indicates that $\Delta S = 0$ transitions – although still possible – do not play a dominant role in the relaxation process.

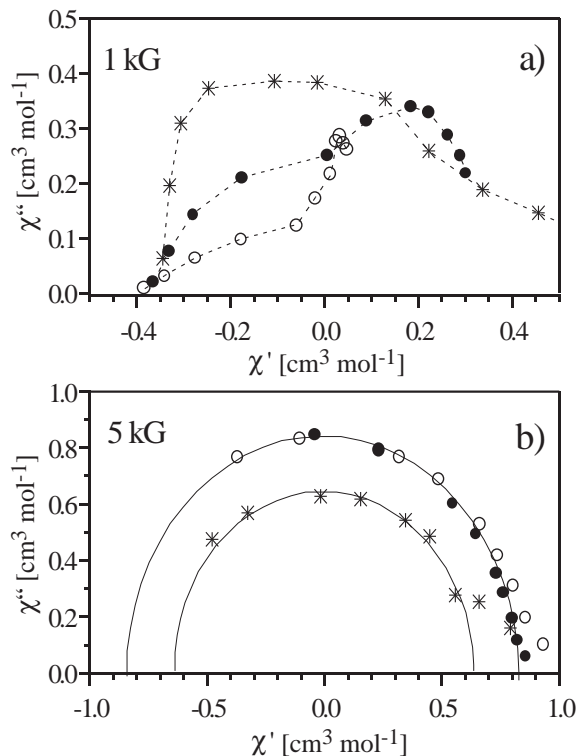


FIG. 10: Argand or Cole-Cole plots of χ'' vs χ' at $H_{DC} = 1$ (a) and 5 kG (b) at fixed temperatures (*, 3.0 K; ●, 4.0 K; ○, 5.0 K). For clarity the data are shifted along the x axis. For a single relaxation process the data points should lie on a semicircle (solid lines) at each temperature.

Fig. 10a shows the so-called Cole-Cole or Argand plot for the AC susceptibility data at $H_{DC} = 1$ kG, in which χ'' is plotted vs χ' for all frequencies at fixed temperatures as indicated. Importantly, for a given temperature the data do not lie on a semicircle but deviate widely,³³ thus unambiguously indicating the presence of a multitude of relaxation processes with different rates. These rates can be calculated using Pauli's master equation in conjunction with Fermi's golden rule, and are obtained as the eigenvalues of the matrix of transition rates.^{23,34,35,36,37} The smallest nonzero eigenrate corresponds to the rate at which the relative populations of both wells reach mutual equilibrium, i.e. to the relaxation of the spin system over the barrier. All the faster rates are associated with transitions between levels inside each of the two wells. In Mn_{12} , e.g., the smallest relaxation rate is about four orders of magnitude smaller than the second-smallest.²³ Consequently, Mn_{12} relaxes with a single observable relaxation rate. Obviously, for Fe_2 the situation is different. The small energetic spread of individual spin-phonon transitions leads to a very narrow distribution of eigenrates that are not resolved experimentally. Therefore, the relaxation phenomenon observed in the AC susceptibility measurements of Fe_2 does not exclusively correspond to the relaxation over the $S = 5/S = 4$ effective energy barrier but also reflects

individual $\Delta S \pm 1$ spin-phonon transitions on either side of this barrier.

At $H_{DC} = 5$ kG the situation is distinctly different. The $1/\tau \propto T$ dependence (Fig. 7) is consistent with a direct rather than an Orbach process, with a spin-phonon transition energy $\hbar\omega < T = 3 - 5$ K.²¹ Also, the Argand plot (Fig. 10b) indicates that $1/\tau$ essentially consists of a single relaxation rate. These results suggest that at 5 kG, the observed relaxation is governed by the transitions between two levels only, which, however, are difficult to identify. Nevertheless, a relaxation process involving the $S = 4$ excited state appears highly unlikely, because (i) at 5 kG the $S = 4$ state has lost its barrier entirely, and (ii) $\hbar\omega \ll T = 3 - 5$ K. Consequently, the monitored relaxation is governed by transitions between two levels of the $S = 5$ state.

The observed increase of χ'' between 1 and 5 kG (Fig. 6, Sec. III C) indicates that the relaxation process becomes increasingly inefficient with H_{DC} . A number of reasons may contribute to this behavior. Perhaps the most important one is that the number of possible spin-phonon transitions involved in the relaxation process shrinks markedly with increasing asymmetry of the potential well, concomitant with a change from an Orbach to a direct relaxation process.

V. SUMMARY AND CONCLUSIONS

This study provides significant insight into the unusual dynamics of the magnetic properties of the spin cluster $[Fe_2F_9]^{3-}$.

First, the observed slow magnetization relaxation in Fe_2 arises from poor thermal contact between the sample and the bath. The resulting phonon bottleneck situation allows for the indirect observation of quantum tunneling of the magnetization through the energy barrier at 1.8 K. Importantly, this result illustrates that a PB situation can provide insight into the dynamics of the spin system at temperatures far above the blocking temperature below which spin-phonon relaxation becomes directly detectable.

Second, in the high-spin system Fe_2 the hysteresis caused by the PB effect adopts a butterfly shape that is phenomenologically analogous to that observed for the low-spin systems V_{15} and Fe_6 . This result indicates that despite the energy barrier in Fe_2 , the spin reversal at $H_z = 0$ occurs much faster than the re-equilibration of the spin+phonons system with the bath. As QTM is rather inefficient in Fe_2 , it further suggests that thermal activation is competitive in achieving spin reversal. Our microscopic model based on the rapid absorption/emission of resonant phonons allows for an accurate reproduction of the hysteresis curves observed for Fe_2 .

Third, AC susceptibility experiments unobstructed by the phonon bottleneck allow for direct insight into spin-phonon dynamics. Even on the timescale of our AC experiments, Fe_2 does not behave as an SMM at $T \geq 1.8$ K.

At $H_{\text{DC}} = 1$ kG an out-of-phase susceptibility is detected with a frequency dependence closely resembling the one typically observed for SMMs; however, the situation in Fe_2 is substantially more complex and highly unusual. The $S = 5$ ground and the $S = 4$ first excited states form a combined system in which the relaxation occurs over the barrier of the combined system, favored by the much higher density of states for thermal phonons suitable for $\Delta S = \pm 1$ than $\Delta S = 0$ transitions. Importantly, this result demonstrates that the measured kinetic energy barrier can actually be *larger* than the thermodynamic barrier of the ground state if the excited state becomes thermally accessible. This result provides an additional twist for the interpretation of the kinetic energy barrier of single-molecule magnets derived from AC susceptibility measurements.

Acknowledgments

The authors thank Stefan Ochsenbein for his aid in performing some of the magnetic measurements, and Dr. Oliver Waldmann for insightful discussions. This work has been supported by the Swiss National Science Foundation and by the TMR program Quemolna of the EU.

APPENDIX

Eq. (7) is derived from Eq. (6) as follows. Generalizing the rotating wave approximation,³⁸ the Hamiltonian in Eq. (6) can be approximated by

$$\mathcal{H}_{\text{eff}} \approx \begin{bmatrix} 25D & h_{5,4} & 0 & \cdots & 0 \\ h_{4,5} & 16D & h_{4,3} & \ddots & \vdots \\ 0 & h_{3,4} & 9D & \ddots & 0 \\ \vdots & \ddots & \ddots & \ddots & h_{-4,-5} \\ 0 & \cdots & 0 & h_{-5,-4} & 25D \end{bmatrix} + g\mu_B H_z \hat{S}_z, \quad (\text{A.1})$$

where $h_{M+1,M} = g\mu_B H_{\text{eff},x} \sqrt{(S-M)(S+M+1)} e^{i\omega_{M+1,M}t}/2$ and $h_{M,M+1} = h_{M+1,M}^*$. To remove the time dependence of Hamiltonian (A.1), a unitary transformation U is applied to Eq. (A.1). In order to obtain the transformation of \mathcal{H}_{eff} to the generalized rotating frame, U has to be applied to the time-dependent Schrödinger equation

$$i\hbar \frac{\partial |\psi\rangle}{\partial t} = \mathcal{H}_{\text{eff}} |\psi\rangle. \quad (\text{A.2})$$

We define the quantum state in the generalized rotating frame by $|\psi_{\text{grot}}\rangle = U |\psi\rangle$. The transformation of the left and right hand side of Eq. (A.2) then yields

$$i\hbar \frac{\partial |\psi\rangle}{\partial t} = i\hbar \left(U^{-1} \frac{\partial |\psi_{\text{grot}}\rangle}{\partial t} + \frac{\partial U^{-1}}{\partial t} |\psi_{\text{grot}}\rangle \right),$$

$$\mathcal{H}_{\text{eff}} |\psi\rangle = \mathcal{H}_{\text{eff}} U^{-1} |\psi_{\text{grot}}\rangle. \quad (\text{A.3})$$

Combining the left and right hand side of Eq. (A.3) leads to

$$i\hbar \left(U^{-1} \frac{\partial |\psi_{\text{grot}}\rangle}{\partial t} + \frac{\partial U^{-1}}{\partial t} |\psi_{\text{grot}}\rangle \right) = \mathcal{H}_{\text{eff}} U^{-1} |\psi_{\text{grot}}\rangle. \quad (\text{A.4})$$

Multiplying Eq. (A.4) by U from the left results in

$$i\hbar \frac{\partial |\psi_{\text{grot}}\rangle}{\partial t} = \left(U \mathcal{H}_{\text{eff}} U^{-1} - i\hbar U \frac{\partial U^{-1}}{\partial t} \right) |\psi_{\text{grot}}\rangle$$

$$\equiv \mathcal{H}_{\text{eff}}^{\text{grot}} |\psi_{\text{grot}}\rangle, \quad (\text{A.5})$$

from which we can directly read off the transformed Hamiltonian

$$\mathcal{H}_{\text{eff}}^{\text{grot}} = U \mathcal{H}_{\text{eff}} U^\dagger - i\hbar U \frac{\partial U^\dagger}{\partial t} = U \mathcal{H}_{\text{eff}} U^\dagger + i\hbar \frac{\partial U}{\partial t} U^\dagger. \quad (\text{A.6})$$

We now choose the following unitary transformation:

$$U = \sum_{M=-5}^5 |M\rangle \langle M| e^{-i\omega_M t}. \quad (\text{A.7})$$

Evaluating $\mathcal{H}'_{\text{eff}} = U \mathcal{H}_{\text{eff}} U^\dagger$ yields

$$\mathcal{H}'_{\text{eff}} = \begin{bmatrix} 25D & h'_{5,4} & 0 & \cdots & 0 \\ h'_{4,5} & 16D & h'_{4,3} & \ddots & \vdots \\ 0 & h'_{3,4} & 9D & \ddots & 0 \\ \vdots & \ddots & \ddots & \ddots & h'_{-4,-5} \\ 0 & \cdots & 0 & h'_{-5,-4} & 25D \end{bmatrix} + g\mu_B H_z \hat{S}_z, \quad (\text{A.8})$$

where $h'_{M+1,M} = h_{M+1,M} e^{i(\omega_M - \omega_{M+1})t}$ and $h'_{M,M+1} = h_{M+1,M}^*$. Setting $\omega_{M+1,M} - \omega_{M+1} + \omega_M = 0$ eliminates the time dependence of

$$\mathcal{H}_{\text{eff}}^{\text{grot}} = \mathcal{H}'_{\text{eff}} + i\hbar \frac{\partial U}{\partial t} U^\dagger$$

$$= g\mu_B H_{\text{eff},x} \hat{S}_x + g\mu_B H_z \hat{S}_z. \quad (\text{A.9})$$

* Electronic address: ralph.schenker@iac.unibe.ch

† Present address: Department of Physics, University of California San Diego, 9500 Gilman Drive, La Jolla, CA 92093-0360; Electronic address: mleuenbe@physics.ucsd.edu

‡ Present address: Laboratoire Léon Brillouin (LLB-CNRS-CEA), CEA Saclay, 91191 Gif-sur-Yvette Cedex, France; Electronic address: chabouss@llb.saclay.cea.fr

§ Electronic address: daniel.loss@unibas.ch

- [¶] Electronic address: hans-ulrich.guedel@iac.unibe.ch
- ¹ M. N. Leuenberger, D. Loss, *Nature* **410**, 789 (2001).
- ² R. Sessoli, D. Gatteschi, A. Caneschi, M. A. Novak, *Nature* **365**, 141, (1993).
- ³ L. Thomas, F. Lioni, R. Ballou, D. Gatteschi, R. Sessoli, B. Barbara, *Nature* **12**, 145 (1996).
- ⁴ J. R. Friedman, M. P. Sarachik, J. Tejada, R. Ziolo, *Phys. Rev. Lett.* **76**, 3830 (1996).
- ⁵ J. M. Hernandez, X. X. Zhang, F. Luis, J. Tejada, J. R. Friedman, M. P. Sarachik, R. Ziolo, *Phys. Rev. B* **55**, 5858 (1997).
- ⁶ C. Sangregorio, T. Ohm, C. Paulsen, R. Sessoli, D. Gatteschi, *Phys. Rev. Lett.* **78**, 4645 (1997).
- ⁷ S. M. J. Aubin, N. R. Dilley, L. Pardi, J. Krzystek, M. W. Wemple, L.-C. Brunel, M. B. Maple, G. Christou, D. N. Hendrickson, *J. Am. Chem. Soc.* **120**, 4991 (1998).
- ⁸ Y. Shapira, M. T. Liu, S. Foner, C. E. Dubé, and P. J. Bonitatebus, Jr., *Phys. Rev. B* **59**, 1046 (1999).
- ⁹ I. Chiorescu, W. Wernsdorfer, A. Müller, H. Bögge, and B. Barbara, *Phys. Rev. Lett.* **84**, 3454 (2000).
- ¹⁰ O. Waldmann, R. Koch, S. Schromm, P. Müller, I. Bernt, and R. W. Saalfrank, *Phys. Rev. Lett.* **89**, 246401 (2002).
- ¹¹ Y. Inagaki, T. Asano, Y. Ajiro, Y. Narumi, K. Kindo, A. Cornia, and D. Gatteschi, *J. Phys. Soc. Japan* **72**, 1178 (2003).
- ¹² Such systems, however, possess an energy barrier for the reversal of the Néel vector orientation, see e.g. M. N. Leuenberger, F. Meier, and D. Loss, *Monatshefte für Chemie* **134**, 217 (2003).
- ¹³ C. Bosovic, W. Wernsdorfer, K. Folting, J. C. Huffman, D. N. Hendrickson, G. Christou, *Inorg. Chem.* **41**, 5107 (2002).
- ¹⁴ R. Schenker, H. Weihe, H. U. Güdel, *Inorg. Chem.* **40**, 4319 (2001).
- ¹⁵ R. Schenker, M. N. Leuenberger, G. Chaboussant, H. U. Güdel, D. Loss, *Chem. Phys. Lett.* **358**, 413 (2002).
- ¹⁶ K. Krämer, R. Schenker, J. Hauser, H. B. Weihe, H. U. Güdel, H.-B. Bürgi, *Z. Anorg. Allg. Chem.* **627**, 2511 (2001).
- ¹⁷ As our SQUID magnetometer does not allow for continuous detection of the magnetic moment upon sweeping the field, the reported sweeping rates Γ are time-averaged and depend on the number of data points within a certain magnetic field interval. The value of $\Gamma \approx 3$ G/s reported for the butterfly loops actually reads $\Gamma = 2.5$ G/s for $0 \leq |H_z| \leq 5$ kG and 3.5 G/s for $|H_z| > 5$ kG.
- ¹⁸ The $[\text{Fe}_2\text{F}_9]^{3-}$ dimer molecules are aligned along $\mathbf{H}_{AC} \parallel \mathbf{H}_{DC} \parallel c$ in the crystal, while they are isotropically oriented in the polycrystalline sample. This difference results in a much larger number of spins not being able to adiabatically follow the oscillating field in the single crystal, leading to a more intense and sharper χ'' signal.
- ¹⁹ J. H. Van Vleck, *Phys. Rev.* **59**, 724 (1941).
- ²⁰ V. Bindilatti, T. Q. Vu, and Y. Shapira, *Solid State Commun.* **77**, 423 (1991).
- ²¹ A. Abragam and B. Bleaney, *Electron Paramagnetic Resonance of Transition Ions*, Clarendon Press: Oxford, 1970, chapter 10.
- ²² I. Chiorescu, W. Wernsdorfer, A. Müller, S. Miyashita, and B. Barbara, *Phys. Rev. B* **67**, 020402(R) (2003).
- ²³ M. N. Leuenberger, D. Loss, *Phys. Rev. B* **61**, 1286 (2000).
- ²⁴ M. N. Leuenberger, D. Loss, M. Poggio, and D. D. Awschalom, *Phys. Rev. Lett.* **89**, 207601/1, (2002).
- ²⁵ M. N. Leuenberger, *J. Mag. Mag. Mat.* **272-276**, 1974 (2004).
- ²⁶ Note that the definition of τ_n is only strictly valid at $H_z = 0$. However, it remains a valid approximation for small magnitudes of H_z .
- ²⁷ M. N. Leuenberger, D. Loss, *Phys. Rev. B* **61**, 12200 (2000).
- ²⁸ J. A. Giordmaine, L. E. Alsop, F. R. Nash, and C. H. Townes, *Phys. Rev.* **109**, 302 (1958).
- ²⁹ P. L. Scott and C. D. Jeffries, *Phys. Rev.* **127**, 32 (1962).
- ³⁰ S. L. Castro, Z. Sun, C. M. Grant, J. C. Bollinger, D. N. Hendrickson, G. Christou, *J. Am. Chem. Soc.* **120**, 2365 (1998).
- ³¹ M. A. Novak and R. Sessoli, In *Quantum Tunneling of Magnetization*; L. Gunther, B. Barbara, Eds.; Kluwer: Dordrecht, p. 171 (1995).
- ³² F. Luis, J. Bartolomé, J. F. Fernández, J. Tejada, J. M. Hernández, X. X. Zhang, and R. Ziolo, *Phys. Rev. B* **55**, 11448 (1997).
- ³³ Varying contributions from $\Delta S = 0$ and $\Delta S = \pm 1$ transitions may have a significant impact on the appearance of the Argand diagram. Notably, while the Arrhenius analysis focuses on the situation at the maximum of the χ'' profiles in Fig. 6, the Argand diagram plots also χ'' values from the wings of these profiles.
- ³⁴ J. Villain, F. Hartman-Boutron, R. Sessoli, and A. Rettori, *Europhys. Lett.* **27**, 159 (1994).
- ³⁵ F. Hartmann-Boutron, P. Politi, and J. Villain, *Int. J. Mod. Phys. B* **10**, 2577 (1996).
- ³⁶ A. Fort, A. Rettori, J. Villain, D. Gatteschi, and R. Sessoli, *Phys. Rev. Lett.* **80**, 612 (1998).
- ³⁷ J. F. Fernández, F. Luis, J. Bartolomé, *Phys. Rev. Lett.* **80**, 5659 (1998).
- ³⁸ J. J. Sakurai, *Modern Quantum Mechanics* (Addison-Wesley, 1994).